Physics of the Earth and Planetary Interiors 189 (2011) 1–8

Contents lists available at SciVerse ScienceDirect

Physics of the Earth and Planetary Interiors

journal homepage: www.elsevier.com/locate/pepi

Lithosphere–asthenosphere viscosity contrast and decoupling

Carlo Doglioni [a], Alik Ismail-Zadeh [b,c,d], Giuliano Panza [e,f], Federica Riguzzi [g,*]

[a] Dipartimento di Scienze della Terra, Università Sapienza, Roma, Italy
[b] Geophysikalisches Institut, Karlsruher Institut für Technologie, Karlsruhe, Germany
[c] International Institute of Earthquake Prediction Theory and Mathematical Geophysics, Russian Academy of Science, Moscow, Russia
[d] Institut de Physique du Globe, Paris, France
[e] Dipartimento di Geoscienze, Università di Trieste, Italy
[f] Abdus Salam International Centre for Theoretical Physics, Trieste, Italy
[g] Istituto Nazionale di Geofisica e Vulcanologia, Roma, Italy

ARTICLE INFO

Article history:
Received 26 May 2011
Received in revised form 15 September 2011
Accepted 16 September 2011
Available online 22 September 2011
Edited by Kei Hirose

Keywords:
Lithosphere dynamics
Asthenosphere
Viscosity contrast
Decoupling
Analytical modelling
Rayleigh–Taylor instability

ABSTRACT

The coupling/decoupling between the lithosphere and asthenosphere has significant implications for understanding many important aspects of plate tectonics and geodynamics. To drive plate motion, mantle convection requires coupling at the lithosphere–asthenosphere (LA) interface. Meanwhile a low viscosity layer in the asthenosphere is indicative of possible LA decoupling. Here we present an analytical model of a stratified uppermost mantle structure disturbed by a long-wavelength perturbation (such as the body tide) to analyse the influence of LA viscosity contrast on the growth (or decay) rates of the perturbation. We show that the viscosity contrast of 8–10 orders of magnitude would allow a relative motion of the lithosphere over the asthenosphere due to the long-wavelength perturbations at the rate of about 10 cm yr^{-1}. These constrains on the viscosity contrast can allow to discriminate between the LA coupling and decoupling. The growing seismic and mineralogical evidences of a possible ultra low viscosity asthenospheric layer may be indicative of the LA decoupling and their relative motions due to long-wavelength perturbations, and a contribution of the tidal drag on the plate motion should not be neglected in the regions of high viscosity contrasts.

1. Introduction

A number of evidences support the hypothesis of significant variations of viscosity in the uppermost mantle. Earth's models based on seismic *P*- and *S*-waves tomography show that the asthenosphere is stratified and laterally heterogeneous (e.g., Thybo, 2006; Panza et al., 2010). In its uppermost part, between 100 and 200 km of depth, the asthenosphere (or the low-velocity anisotropic layer, Anderson, 2010) contains a well-developed low-velocity zone, LVZ (e.g., Dziewonski and Anderson, 1981), where the velocity decrease of *S*-waves is larger than that of *P*-waves, indicating the presence of a significant amount of melt. This is often interpreted being related to the hotter geotherm than the mantle solidus at 150–200 km depth (Fig. 1). However the melting can be favoured by a more abundant presence of free water in the pressure range from 3 to 6 GPa, i.e., 100–200 km depth (Green et al., 2010). In addition, electromagnetic studies support the presence of a thin asthenospheric layer with significant amount of fluids (Calcagnile and Panza, 1987; Adám and Panza, 1989; Heinson, 1999) that would drop the viscosity of the LVZ.

The lithosphere–asthenosphere (LA) transition is considered to be a zone of decoupling (e.g., Craig and McKenzie, 1986; Doglioni et al., 2005; Anderson, 2010 and references therein). The decoupling at the base of the lithosphere has been postulated in order to satisfy the geoid anomaly across transform zones (Craig and McKenzie, 1986). An ultra-thin velocity anisotropy zone in the asthenosphere has been detected by Marone and Romanowicz (2007), and shear heating in the decoupling zone (Doglioni et al., 2005) can determine a super-adiabatic condition in the low-velocity layer (Anderson, 2010).

The post-glacial rebound (PGR) analysis can provide important constraints on mantle viscosity structure. Using synthetic PGR data calculated for an Earth model with the realistic 3-D viscosity structure (based on seismic tomography models) and constrained by relative sea levels, exponential relaxation times, polar wander, GRACE time-variable gravity measurements and some other observations, Paulson et al. (2007) showed that an inversion for a 1-D (spherically symmetric) two-layered viscosity structure (upper and lower mantle) provides well-constrained values, which correspond to the two-layer average of the logarithm of their 3-D viscosity structure. Meanwhile using four-layered viscosity structure of the Earth, the authors found that neighbouring layers may have highly variable viscosities while maintaining a constant

* Corresponding author.
E-mail address: federica.riguzzi@ingv.it (F. Riguzzi).

0031-9201/$ - see front matter © 2011 Elsevier B.V. All rights reserved.
doi:10.1016/j.pepi.2011.09.006

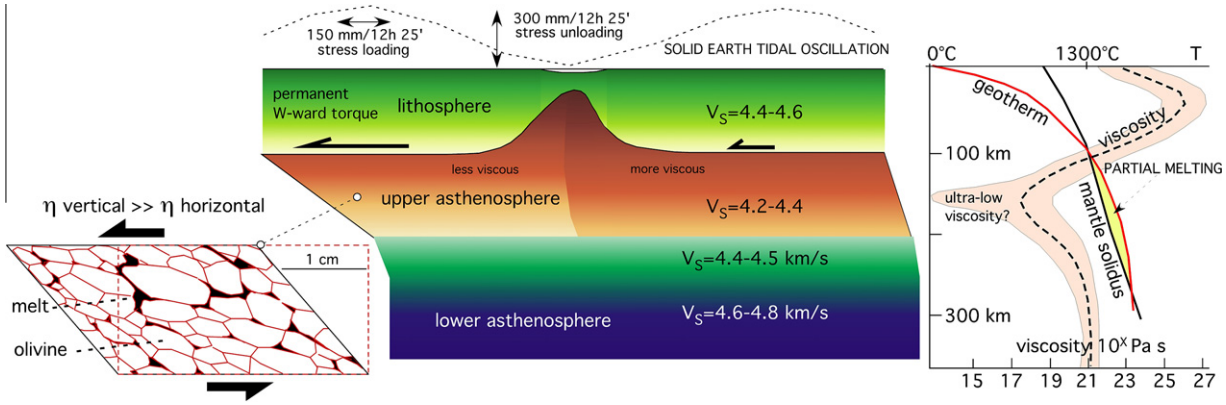

Fig. 1. The lithosphere, asthenosphere and underlying upper mantle (marked by variable shear wave velocity). Central panel: stratigraphy and shear wave velocities (Vs) of the lithosphere–asthenosphere (LA) transition. Solid Earth's tides keep the system permanently oscillating. The asthenosphere is inferred as the main decoupling zone of the lithosphere relative to the underlying mantle. Right panel: average viscosity (dashed line) and possible ranges of viscosity variation (light grey). The upper asthenosphere, also called low-velocity zone (LVZ), is characterized by partial melting. Left panel: having some intergranular melt, the olivine crystals may roll laterally when subject to horizontal shear. Therefore, the viscosity (η) of the asthenosphere can be of a few orders of magnitude lower when measured under horizontal shear with respect to vertical loading or unloading, being this value still unknown.

average between them and concluded that that the PGR data remain unable to constrain multiple viscosity layers within the upper mantle.

A PGR analysis cannot reveal a relatively thin low viscosity layer hosted in the asthenospheric low-velocity mantle (Scoppola et al., 2006). The theory of the channel flow (Cathles, 1975) shows how a thin (e.g., a few tens of km) low viscosity layer in the asthenosphere remains unsolved or invisible in the PGR computation due to the much deeper effect of a 1000 km wide ice cap loading. Therefore, the asthenospheric channel cannot contribute significantly to isostatic subsidence or uplift induced by widely distributed loading or unloading of the lithosphere. It would be much easier to deform the entire upper mantle, even if it has a much higher average viscosity. This implies the limit of the glacial isostatic rebound studies in determining the asthenospheric viscosity.

Moreover, these upper mantle layers are beyond the reach of standard seismic tomography due to the limitations of the theoretical framework employed; ray theory does not handle diffraction and frequency dependence, whereas normal mode perturbation theory requires weak and smooth lateral variations of structure (e.g., Waldhauser et al., 2002; Romanowicz, 2003; Anderson, 2007; Boschi et al., 2007; Panza et al., 2007b; Ismail-Zadeh et al., 2010). In the asthenosphere, the horizontally polarized shear waves travel faster than vertically, suggesting a horizontal unidirectional distribution of the olivine crystals, supporting a shear within this layer (Fig. 1). This anisotropy has been related to horizontal shear in the low-viscosity asthenosphere (Bokelmann, 2002), which is thinner below the continents than beneath the oceans (Gung et al., 2003; Panza et al., 2010).

Petrological and laboratory experiments are in favour of very low viscosity in the asthenosphere, particularly when intra-crystal pockets of melt occur (Hirth and Kohlstedt, 1995; Holtzman et al., 2003; Dingwell et al., 2004; Liebske et al., 2005). Laboratory experiments suggest that the viscosity of the asthenosphere could be significantly heterogeneous. Both water and melt content of asthenospheric rocks can influence their viscosity (Hirth and Kohlstedt, 1996; Mei et al., 2002). The viscosity of the upper asthenosphere should be drastically lower if the LVZ is vapour saturated, increasing the partial melting of a lherzolitic mantle as recently shown by Green et al. (2010). An effective viscosity of the asthenosphere can be significantly influenced by a water content lowering its viscosity to 10^{15} Pa s in the case of both diffusion and dislocation creeps (Korenaga and Karato, 2008). Moreover, the viscosity in the asthenospheric LVZ can be even three orders of magnitude lower when measured under horizontal shear (Fig. 1) with respect to the viscosity computed by vertical unloading due to post-glacial rebound (Scoppola et al., 2006). In fact, Jin et al. (1994) showed how the intra-crystalline melt in the asthenospheric peridotites under shear (Stevenson, 1994) could generate a viscosity of about 10^{12} Pa s. These very low values require the presence of high melt fractions (Hirth and Kohlstedt, 2003; Kohlstedt and Holtzman, 2009; Kohlstedt et al., 2010), which is compatible with a hotter than expected asthenosphere (Anderson, 2010) and the low values of radial anisotropy in the LVZ (Panza et al., 2010).

The fastest moving plate both in the no-net rotation and in the hotspot reference frames (i.e., the Pacific, Crespi et al., 2007) has the lowest viscosity value estimated so far from the modelling of earthquake remote triggering (Pollitz et al. 1998). This indicates that the viscosity of the LVZ in the upper asthenosphere (Fig. 1) controls the velocity of the lithosphere relative to the asthenosphere, i.e., the amount of decoupling. Therefore, the higher the viscosity of the asthenosphere, the smaller the decoupling between the lithosphere and the asthenosphere and the slower the velocity of the plate. Then lateral variations in asthenosphere viscosity should determine velocity gradients in the overlying lithosphere, i.e., plates interaction (Doglioni, 1993). Mantle convection should redistribute over the time these lateral anisotropies.

In this paper we use an analytical model to study the influence of LA viscosity contrast on the plate movements and to analyse how a long-wavelength perturbation of the LA system can allow the decoupling at rates comparable to those inferred from geological and geophysical data.

2. A model of lithosphere–asthenosphere dynamics under long-wavelength perturbations

The Earth's dynamics is characterized by thermal convection in the mantle and conductive heat transfer in the lithosphere, which is considered to be the upper thermal boundary layer of mantle convection. This requires the lithosphere to be cooler than the underlying asthenosphere. The lithosphere behaves then as an elastic rigid body for short-time scales and as a visco-plastic body (or a perfectly plastic fluid) at geological time scales.

The influence of the LA viscosity contrast on the growth rates of small long-wavelength perturbations of the LA structure is analysed here using the theory of gravitational (Rayleigh–Taylor, RT) instability. This approach reduces the non-linear problem of LA

dynamics to a linearised problem, which allows for analytic solutions and provides useful physical insight into the dynamics of the LA structure. The RT theory should eventually fail, as perturbations grow to large amplitudes with time and the non-linear terms in the governing equations become large. Nevertheless the theory can capture the initial dynamics of the LA structure and provide simplicity to a complex process. The modelling provides a theoretical framework for the analysis of the lithosphere dynamics with respect to the underlying low-viscosity asthenosphere and for the study of the growth of long-wavelength perturbations of the lithosphere like those due to tidal waves.

2.1. Mathematical statement of the problem

We consider a simplified model of the uppermost mantle (Fig. 2) consisting of the lithosphere (the upper layer), the asthenosphere (the middle layer), and the sub-asthenospheric mantle (the lower layer). A perfectly plastic layer $0 \leqslant z \leqslant h_1$ (h_1 = 120 km) with effective viscosity η_1 and density ρ_1 simulates the lithosphere. This layer overlays a layer of viscous fluid $-h_2 \leqslant z \leqslant 0$ (h_2 = 60 km) with viscosity η_2 and density ρ_2. Both layers (lithosphere and asthenosphere) rest on an infinitely thick layer filled by a non-Newtonian power-law fluid with effective viscosity η_3 and density ρ_3. Hereinafter subscripts 1, 2, and 3 refer to the upper, middle, and lower layers, respectively.

The governing equations are represented by the equations of momentum, rheology, continuity, and density advection for small perturbations of physical variables (e.g., Ismail-Zadeh, 1994; Ismail-Zadeh and Tackley, 2010). Motivated by the extremely large viscosities of geological fluids, we assume that the inertial terms in the Navier–Stokes equations are negligible and that the motion is governed by Stokes equations. In general, the stress tensor τ_{ij} and strain rate tensor $\dot{\varepsilon}_{ij}$ are linked by the non-Newtonian fluid power-law $\tau_{ij} = C\dot{\varepsilon}^{(1-n)/n}\dot{\varepsilon}_{ij}$, where the constant C is defined from the thermodynamical conditions, n is the power-law exponent, and $\dot{\varepsilon} = (\dot{\varepsilon}_{kl}\dot{\varepsilon}_{kl})^{1/2}$ is the second invariant of the strain rate. The structure is subject to layer-parallel motion inducing the horizontal background flow with strain rates $\dot{\bar{\varepsilon}}_{xx} = \pm\gamma_1$ in the upper layer and $\dot{\bar{\varepsilon}}_{xx} = \pm\gamma_2$ in the lower layer, where γ_1 and γ_2 are constants. Incompressibility implies that $\dot{\bar{\varepsilon}}_{zz} = -\dot{\bar{\varepsilon}}_{xx}$. The remaining component of the strain rate tensor $\dot{\bar{\varepsilon}}_{xz}$ equals zero for the background pure shear flow.

In order to obtain the equations governing the small perturbations of the physical variables, we neglect all products and powers of the perturbations and retain only linear terms. We introduce small perturbations of pressure (δP), density ($\delta\rho$), components of velocity $\mathbf{v} = (u, w)$, stress tensor ($\delta\tau_{ij}$), and strain-rate tensor ($\delta\dot{\varepsilon}_{ij}$). The governing equations take then the form

$$-\frac{\partial\delta P}{\partial x} + \frac{\partial\delta\tau_{xx}}{\partial x} + \frac{\partial\delta\tau_{xz}}{\partial z} = 0, \tag{1}$$

$$-\frac{\partial\delta P}{\partial z} + \frac{\partial\delta\tau_{xz}}{\partial x} + \frac{\partial\delta\tau_{zz}}{\partial z} = g\delta\rho, \tag{2}$$

$$\delta\tau_{xx} = 2\frac{\bar{\eta}}{n}\frac{\partial u}{\partial x}, \quad \delta\tau_{zz} = 2\frac{\bar{\eta}}{n}\frac{\partial w}{\partial z}, \quad \delta\tau_{xz} = \bar{\eta}\left(\frac{\partial u}{\partial z} + \frac{\partial w}{\partial x}\right) \tag{3}$$

$$div\mathbf{v} = 0, \tag{4}$$

$$\frac{\partial\delta\rho}{\partial t} + w\frac{d\rho}{dz} = 0, \tag{5}$$

where $\bar{\eta}$ is the effective viscosity defined as $\bar{\eta} = 0.5C\dot{\bar{\varepsilon}}^{\frac{1-n}{n}}$. Eq. (3) represent the anisotropic stress–strain rate relationships in the case of non-Newtonian power-law rheology (e.g., Fletcher, 1974; Ismail-Zadeh et al., 2002).

The conditions at the upper boundary ($z = h_1$) are stress-free and are obtained from the absence of tangential and normal stress

$$\delta\tau_{xz,1} = \bar{\sigma}_{xx,1}\frac{\partial\zeta}{\partial x}, \tag{6}$$

$$-\delta P_1 + \delta\tau_{zz,1} + \rho_1 g\zeta = 0, \tag{7}$$

where $\bar{\sigma}_{xx,1} = 4\eta_1\dot{\bar{\varepsilon}}_{xx,1} = 4\eta_1\gamma$ is the component of the stress tensor for the basic background flow (Smith, 1979), and ζ is the vertical displacement of the upper boundary defined by $\partial\zeta/\partial t = w_1$.

At the interfaces between the upper and middle layers ($z = 0$) and the middle and lower layers ($z = -h_2$), we require the continuity of velocity, tangential and normal stress accounting for the forces due to the density and viscosity discontinuities at the interface

$$u_i = u_{i+1}, \quad w_i = w_{i+1}, \tag{8}$$

$$\delta\tau_{xz,i} - \delta\tau_{xz,i+1} = (\bar{\sigma}_{xx,i} - \bar{\sigma}_{xx,i+1})\frac{\partial\xi_i}{\partial x} \tag{9}$$

$$-\delta P_i + \delta P_{i+1} + \delta\tau_{zz,i} - \delta\tau_{zz,i+1} - (\rho_{i+1} - \rho_i)g\xi_i = 0 \tag{10}$$

where $\partial\xi_i/\partial t = w_i = w_{i+1}$ and i = 1,2. Eqs. (6) and (9) include the driving mechanism for the background flow, while the last term in (7) and (10) provides the motion of the layered structure due to density discontinuity.

2.2. Linearised problem

In order to analyse the disturbance to the normal modes of the model, the Laplace-Fourier transform is used with the kernel $\exp(ikx + pt)$, where k is the wave-number and p is the growth rate of the perturbations, and the stability problem then reduces to the analysis of the variable p as a function of k. For solutions having the assumed dependence on x and t, the set of Eqs. (1)–(5) can be transformed into the ordinary differential equation of the fourth order (see Appendix 1):

$$(D^2 + k^2)^2 w - \frac{4k^2}{n}D^2 w = 0. \tag{11}$$

The general solution of (11) has the form

$$w = A_3\exp(k\beta_1 z) + B_3\exp(k\beta_2 z) + C_3\exp(k\beta_3 z) + D_3\exp(k\beta_4 z), \tag{12}$$

where

$$\beta_j = \pm\left[\frac{2}{n} - 1 \pm \frac{2(1-n)^{1/2}}{n}\right]^{1/2}, \quad j = 1,2,3,4. \tag{13}$$

For a *Newtonian viscous fluid* (n = 1) Eq. (11) becomes

$$(D^2 - k^2)^2 w = 0 \tag{14}$$

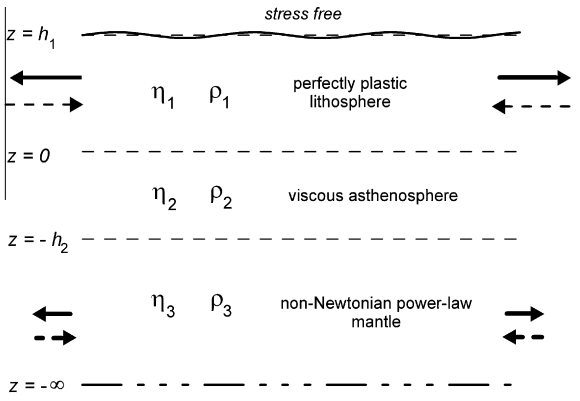

Fig. 2. A model sketch of the lithosphere/asthenosphere structure. A small long-wavelength perturbation is prescribed to the stress free surface. Solid and dashed arrows indicated that the structure is subject to background horizontal flow.

with the general solution

$$w = A_2 \cosh kz + B_2 \sinh kz + C_2 z \cosh kz + D_2 z \sinh kz. \quad (15)$$

For a *perfectly plastic fluid* ($n \to \infty$) Eq. (11) becomes

$$(D^2 + k^2)^2 w = 0 \quad (16)$$

with the general solution

$$w = A_1 \cos kz + B_1 \sin kz + C_1 z \cos kz + D_1 z \sin kz, \quad (17)$$

where A_i, B_i, C_i, and D_i ($i = 1,2,3$) in Eqs. (12), (15), and (17) are constants.

Boundary conditions (6)–(10) have the form:

$$\left(D^2 + k^2 - \frac{4\gamma_1 k^2}{p}\right) w_1 = 0, \quad (18)$$

$$\left(D + \frac{1}{k^2} D^3 - \frac{\rho_1 g}{\eta_1 p}\right) w_1 = 0, \quad (19)$$

$$w_1 = w_2, \quad Dw_1 = Dw_2, \quad (20)$$

$$(D^2 + k^2) w_1 = \frac{\eta_2}{\eta_1}(D^2 + k^2) w_2 + \frac{4\gamma_1 k^2}{p}\left(1 - \frac{\eta_2}{\eta_1}\right) w_2, \quad (21)$$

$$\left(\frac{1}{k^2} D^3 + D\right) w_1 - \frac{\eta_2}{\eta_1}\left(\frac{1}{k^2} D^3 - 3D\right) w_2 = \frac{(\rho_1 - \rho_2) g}{\eta_1 p} w_2 \quad (22)$$

$$w_2 = w_3, \quad Dw_2 = Dw_3, \quad (23)$$

$$\frac{\eta_2}{\eta_3}\left(D^2 + k^2\right) w_2 = (D^2 + k^2) w_3 + \frac{2k^2}{p}\left(\gamma_1 \frac{\eta_2}{\eta_3} - \gamma_2\right) w_3, \quad (24)$$

$$\frac{\eta_2}{\eta_3}\left(\frac{1}{k^2} D^3 - 3D\right) w_2 - \left(\frac{1}{k^2} D^3 - \frac{1}{3} D\right) w_3 = \frac{(\rho_2 - \rho_3) g}{\eta_3 p} w_3. \quad (25)$$

Eq. (16) for the upper layer, Eq. (14) for the middle layer, and Eq. (11) for the lower layer ($n = 3$) with boundary conditions (18)–(25) define the boundary value problem for the eigenvalue p and eigenfunction w. The conditions of no flow as $z \to \infty$ reduce the solution (12) to equation (11) to the following form

$$w = \exp(kaz)(A_3 \cos(kbz) + B_3 \sin(kbz)), \quad (26)$$

where $a = \cos\frac{\varphi}{2}$, $b = \sin\frac{\varphi}{2}$, and $\varphi = \arccos(-1/3)$. Substituting solutions (15), (17), and (26) into the boundary conditions (18)–(25), we obtain a system of ten linear algebraic equations for ten constants A_k, B_k, C_l, and D_l ($k = 1,2,3$; $l = 1,2$). Zeros of the determinant of the linear system are eigenvalues of the boundary value problem. Introducing dimensionless quantities, the problem can be reduced to the determination of the growth rate p of small perturbations from a cubic polynomial function (see Appendix 2).

2.3. Model results

Despite the analysis is dimensionless, the results of our modelling are presented here in dimensional units. We consider the following values of the physical parameters in our analytical model. According to the PREM model (Dziewonski and Anderson, 1981), we prescribe the density values to the upper layer (lithosphere), middle layer (asthenosphere), and lower layer (underlying mantle) as $\rho_1 = 3375$ kg m^{-3}, $\rho_2 = 3360$ kg m^{-3}, and $\rho_3 = 3540$ kg m^{-3}, respectively. Hence in the model we assume the density of the lithosphere to be slightly higher than that of the asthenosphere (the density jump is 15 kg m^{-3}). Meanwhile the density jump between the lithosphere and the asthenosphere can be higher: based on geodetic observations of surface displacements induced by ocean tidal loads Ito and Simons (2011) showed that the density jump is about 50 kg m^{-3}.

The typical time scale is $t_0 = 1$ My, and the effective viscosity of the lithosphere and the sub-asthenospheric mantle is assumed to be constant ($\eta_1 = 10^{23}$ Pa s and $\eta_3 = 10^{21}$ Pa s), while the viscosity of the asthenosphere, η_2, varies. Solid Earth tidal waves have a long wavelength, $L = 2\pi/k$, which is latitude-dependent and varies from few thousands km to about 20,000 km. Moreover the interference of the Moon and Sun tides (being the last one about 0.46 that of the Moon), determines variable and shorter wavelengths. To be conservative, we analyse the growth rate of initial perturbations of the lithosphere at long wavelengths, although the maximum growth rate is reached at smaller wavelengths. The dimensional growth rate (cm yr^{-1}) in the LA system, U, is defined as the growth, by a factor of e (2.71828), of the small long-wavelength perturbation s (30 cm) of the lithosphere for the characteristic time: $U = \lambda se/t_0$, where λ is the dimensionless growth rate. The growth rate in the model depends on the wavelength of the perturbation, the viscosity ratio (not on the absolute value of effective viscosity of the lithosphere and of the asthenosphere), the density contrast, the ratio of the layers' thickness, and on the background strain rates. We consider the case when the horizontal background strain rates, γ_1 and γ_2, are so small to prevent the development of the buckling instability. The performed numerical experiments show that $\gamma_0 \approx 10^{-17}$ s^{-1} is a reasonable value for the background strain rate in this case. For small values of the strain rate the gravity plays a dominant part in the instability of the LA structure.

Estimates of the average speed of the net rotation range from less than 4.9 cm yr^{-1} to 13.4 cm yr^{-1} depending on the hot spot reference frame employed in the calculation (Gripp and Gordon, 2002; Crespi et al., 2007; Cuffaro and Doglioni, 2007). We compare our model results with these estimates. Fig. 3 shows the growth rate versus wavelength for various values of the viscosity contrast between the lithosphere and the asthenosphere (the effective viscosity ratio η_1/η_2). We see that, when the effective viscosity ratio is less than 10^8, long-wavelength perturbations grow very slowly at the rate of less than 1 cm yr^{-1}. Meanwhile for larger effective viscosity ratio (e.g., $\eta_1/\eta_2 \geqslant 10^9$), the growth rate of the initial perturbation of the lithosphere falls into the range of the estimated average speed of the net rotation (the grey stripe). The broken lines present the results for the same viscosity ratio but varying thickness ratio between the lithosphere and the asthenosphere. The thicker the asthenosphere layer, the higher growth rate and vice versa. Therefore, if the LA viscosity contrast is small, long-wavelength perturbations will not significantly affect the lithospheric plate motion. However, the perturbations due to tidal drag can influence the plate tectonics processes, if the LA viscosity ratio is

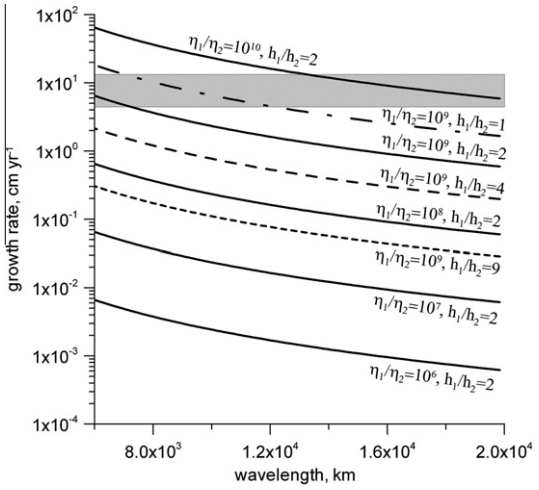

Fig. 3. The growth rate of small perturbations versus wavelength for various values of the effective viscosity ratio (η_1/η_2) at $h_1/h_2 = 2$, $(\rho_1 - \rho_2)/(\rho_1 + \rho_3) = 2.2 \times 10^{-3}$, $(\rho_3 - \rho_2)/(\rho_1 + \rho_3) = 2.6 \times 10^{-2}$, and $\gamma_1 = 10^{-18}$ s^{-1}, $\gamma_2 = 10^{-18}$ s^{-1}. Dashed-dotted, dashed, and dotted lines present the curves of the growth rate for $\eta_1/\eta_2 = 10^9$ and three values of the thickness ratio $h_1/h_2 = 1$, 4, and 9, respectively. The grey stripe indicates the range of the estimated average speed of the net rotation.

larger than eight. Small variations of the viscosity ratio between the asthenospheric and the sub-asthenospheric mantle layers influence insignificantly on the model results.

The maximum growth rates versus the effective viscosity ratio η_1/η_2 are presented in Fig. 4 for three values γ_1 of the background strain rate in the upper layer (lithosphere). The maximum growth rate increases with decreasing effective viscosity ratio and with increasing background strain rate in the lithosphere. At large background strain rates, i.e., for $\gamma_1 > 10^{-14}\,s^{-1}$, the growth rate increases significantly, and the structure tends to a resonant behaviour (Smith, 1979; Ismail-Zadeh et al., 2002). Fig. 4 illustrates that the growth rates of the initial long-wavelength perturbations of the lithosphere fall in the range of the estimates of the average rates of the plate motion at the viscosity contrast between 10^8 and 10^{10} and the background strain rates in the lithosphere between 10^{-17} and $10^{-14}\,s^{-1}$.

The lithosphere and sub-lithospheric mantle are usually modelled as chemically homogeneous layers and with a geotherm increasing with depth. With this assumptions, it has been inferred the convective downwelling of the cold heavier lithosphere into the hotter lighter mantle triggered by the density inversion. However it has been demonstrated the lateral and vertical variety of the chemistry and physical properties of both the lithospheric and asthenospheric mantle (e.g., Anderson, 2006; Panza et al., 2007a). Moreover, xenoliths studies have shown that the lithospheric mantle can be lighter with respect to the asthenosphere (Kelly et al., 2003). To analyse the influence of low density lithosphere on the LA dynamics, we model the case of no density inversion between the lithosphere and the asthenosphere, that is, the density of the asthenosphere is 15 kg m^{-3} higher than that of the lithosphere. In this case small perturbation of the LA structure will not grow but decay. The predicted rate of the decay (Fig. 5) is small compared to the case of density inversion, although it increases with the wavelength of the perturbation and with the viscosity ratio (from less than 10^{-3} to 2×10^{-2} cm yr^{-1}). Nevertheless the rate is insignificant to contribute much to plate tectonics processes.

3. Discussion

Seismic and laboratory studies present growing evidence of a low velocity layer in the upper asthenosphere, which can be

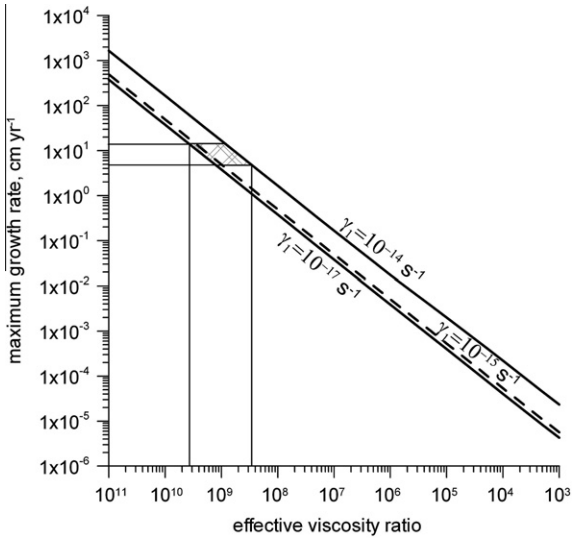

Fig. 4. The maximum growth rate versus the viscosity contrast (effective viscosity ratio η_1/η_2) for three values of the background strain rate in the upper layer (γ_1) at $h_1/h_2 = 2$, $(\rho_1 - \rho_2)/(\rho_1 + \rho_3) = 2.2 \times 10^{-3}$, $(\rho_3 - \rho_2)/(\rho_1 + \rho_3) = 2.6 \times 10^{-2}$, and $\gamma_2 = 10^{-18}\,s^{-1}$.

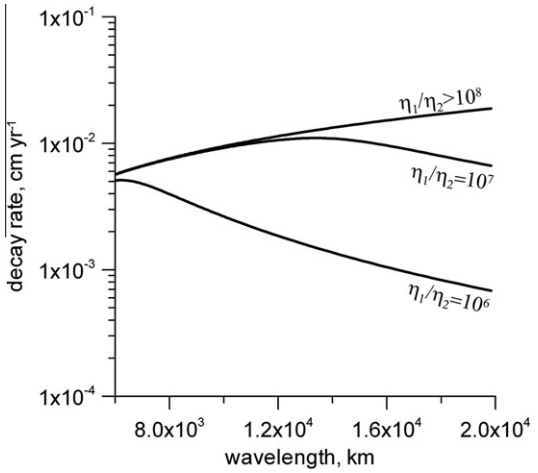

Fig. 5. The decay rate of small perturbations versus wavelength for various values of the effective viscosity ratio (η_1/η_2) at $h_1/h_2 = 2$, $(\rho_1 - \rho_2)/(\rho_1 + \rho_3) = 2.2 \times 10^{-3}$, $(\rho_3 - \rho_2)/(\rho_1 + \rho_3) = 2.4 \times 10^{-2}$, and $\gamma_1 = 10^{-18}\,s^{-1}, \gamma_2 = 10^{-18}\,s^{-1}$.

associated to a water-rich and low-viscosity upper mantle (Jin et al., 1994; Hirth and Kohlstedt, 1995, 1996; Pollitz et al., 1998; Mei et al., 2002; Zandt et al., 2004; Rychert et al., 2005; Green et al., 2010), where decoupling can focus. If a low viscosity channel exists in the upper asthenosphere (LVZ) and may lead to LA decoupling as predicted by the analytical model, it could contribute also to the net rotation of the lithosphere. The lithosphere net rotation with respect to the mantle (e.g., Gripp and Gordon, 2002) implies a relative motion at LA, also known as the westward (W-ward) drift of the lithosphere (Le Pichon, 1968). The origin of the net rotation of the Earth's lithosphere is debated.

There are two competing hypothesis on the kinematics and the mechanism driving the W-ward rotation of the lithosphere relative to the mantle. One hypothesis states that lateral viscosity and density variations in the mantle are suggested to be the primary sources of the net rotation, and the net rotation is only a mean rotation mainly generated by the stronger pull of slabs surrounding the western Pacific. Consequently the faster W-ward velocity of the Pacific plate dominates the global kinematics of plates, giving a W-ward residual to the whole lithosphere (e.g., Ricard et al., 1991; O'Connell et al, 1991). Alternatively, the net rotation is interpreted as a result of rotational drag on the lithosphere due to the tides affecting both the fluid and solid Earth (e.g., Bostrom, 1971; Knopoff and Leeds, 1972; Nelson and Temple, 1972; Moore, 1973). According to the alternative hypothesis, the motion of the lithosphere to the "west" is driven by the concurrent action of Earth's rotation, tidal despinning and mantle convection (e.g., Doglioni et al., 2005; Crespi et al., 2007; Cuffaro and Doglioni, 2007; Riguzzi et al., 2010).

Regardless its origin, the net rotation of the lithosphere indicates some relative motion occurring at the LA transition. Le Pichon (1968) noted that plates and plate boundaries moved toward the west relative to Antarctica. The rate of the net rotation is determined to vary between 0.2° Myr^{-1} (Becker, 2008; Kreemer, 2009) and 1.2° Myr^{-1} (Crespi et al., 2007), depending on the modelling constraints and the adopted reference framework (shear-wave splitting, Pacific hotspots, deep or shallow hotspot reference frame, etc.).

Rotational drag is energetically feasible, because the dissipation of energy by tidal friction balances the energy released by tectonic action (e.g., Riguzzi et al., 2010). Meanwhile Jordan (1974) and Ranalli (2000) argued that the asthenosphere viscosity value estimated from PGR is too high to allow the W-ward decoupling of the lithosphere triggered by the tidal torque. Evidently, a

high-viscosity asthenosphere would not allow a decoupling of the lithosphere driven by the tidal drag. However a thin partially melted low-viscosity layer within the asthenosphere has a little influence on isostasy and on PGR due to the "channel flow effect" (Cathles, 1975; Scoppola et al., 2006). This "invisible" but effective layer could accommodate the relative motion of the lithosphere over the underlying asthenosphere. Our estimations are valid both for a flat or circular topography of LA. Subducting slabs penetrating below the decoupling zone act as anchors in the mantle, resisting to the motion. This is consistent with the lateral migration of slabs that can be inferred by the subduction hinge migration (e.g., Doglioni et al., 2007). Moreover, lateral variations in the LA topography (e.g., deeper under old cratons) will generate different velocity of the decoupling, since, at a given angular velocity, the linear velocity will be function of the length of the radius. Therefore, lateral variations in viscosity in the LVZ and/or variations of the decoupling depth can control, at least partially, the observed different velocities of the overlying lithospheric plates.

The westward net rotation of the lithosphere can account for several tectonic asymmetries recognizable at global scale. Along subduction zones for example, W-directed slabs are steeper with respect to E-NE-directed slabs (e.g., Riguzzi et al., 2010). In fact the subduction zones associated to W-directed slabs have the subduction hinge that moves away (E-ward) relative to the upper plate (Doglioni et al., 2007). The resulting accretionary prisms have low elevation, and they are associated to backarc spreading. On the other hand, the orogens associated to E- or NE-directed slabs, where the subduction hinge converges relative to the upper plate (still generally moving relatively E-ward), rather have high structural and morphological elevation, no typical backarc spreading, and the orogens have double vergence. Even oceanic rifts show a global asymmetric signature as a function of their polarity, where the western limb of rift zones has a slightly deeper bathymetry, and *S*-waves are faster in the lithosphere and slower in the asthenosphere with respect to those of the eastern limb (Panza et al., 2010). The geological record indicates also that this tectonic asymmetry was occurring also in the past, since at least the Palaeozoic (Doglioni, 1993).

4. Conclusion

A simple stratified LA structure has been modelled and analysed, where a low-frequency oscillation such as the body tide is imposed. When the effective viscosity contrast between the lithosphere and the asthenosphere ranges between 10^8 and 10^{10}, the rate of lithospheric motion (e.g., due to solid Earth tides) can range between 1 and 10 cm yr^{-1} thus influencing tectonic processes. The contribution of the tidal drag to the processes weakens with the decrease of the viscosity contrast. The growth rate of the perturbations is enhanced by the increasing background strain rate of the lithosphere. The predicted viscosity contrast between the lithosphere and asthenosphere required to influence the lithosphere dynamics due to tidal drag is consistent with the present knowledge of the ranges between the lithosphere (10^{22}–10^{27} Pa s) and asthenosphere (10^{12}–10^{19} Pa s) viscosities.

Although the analytical model does not consider the permanent W-ward drag acting on the lithosphere, the model predicts the growth rates of the long-wavelength perturbations of the lithosphere to be consistent with the estimates of the average rates of the lithospheric plate movement. If the viscosity contrast between the lithosphere and asthenosphere is high enough, a contribution of the tidal drag to plate motion should not be neglected, and the plate movements should be considered as a combined effect of the thermal convection in the mantle and the tidal drag.

The asthenospheric layer of ultra-low viscosity may evolve in time and space: the viscosity of the layer can decrease or increase depending on the presence of volatiles; and it can become thin or wide depending on the amount of partial melting. Therefore, the LA decoupling and the contribution of the tidal drag depend on the viscosity contrast between the lithosphere and the asthenosphere.

Acknowledgements

Discussions with D. Anderson, E. Bonatti, J.-P. Burg, E. Carminati, M. Cuffaro, K. Fuchs, G. Gallavotti, and F. Innocenti were very stimulating. We thank K. Hirose (Editor), T. Gerya, and an anonymous reviewer for their review and constructive comments. Research supported by DFG IS203/1-1, Miur-Prin 2008, CNR Eurocores, TopoEurope, and RASP Program No. 23.

Appendix A. Linearised constitutive relations

Variables in (1)–(5) are easily separated by the Laplace (in t) and Fourier (in x) transformations. Namely, any desired function f and its transform F are related by

$$F = \frac{1}{2\pi}\int_0^\infty \int_x f(x,z,t)\exp(ikx - pt)dxdt,$$

$$f = \frac{1}{4\pi^2 i}\int_{\sigma-i\infty}^{\sigma+i\infty} \int_k F(k,z,p)\exp(-ikx + pt)dkdp. \quad \text{(A1)}$$

Applying the transformation (A1) to the set of Eqs. (1)–(5) we obtain

$$ik\delta P = -\frac{2\bar{\eta}}{n}k^2 u + D(\bar{\eta}(Du + ikw)), \quad \text{(A2)}$$

$$D\delta P = ik(\bar{\eta}(Du + ikw)) + D\left(\frac{2\bar{\eta}}{n}Dw\right) - g\delta\rho, \quad \text{(A3)}$$

$$iku + Dw = 0, \quad p\delta\rho = -wD\rho, \quad \text{(A4)}$$

where $D = d/dz$. Multiplying (A2) by ik and combining (A3) and (A4) we obtain

$$-k^2\delta P = \frac{2\bar{\eta}}{n}k^2 Dw - D(\bar{\eta}(D^2 + k^2)w), \quad \text{(A5)}$$

$$D\delta P = -\bar{\eta}(D^2 + k^2)w + D\left(\frac{2\bar{\eta}}{n}Dw\right) - g\frac{D\rho}{p}w. \quad \text{(A6)}$$

Finally, eliminating δP between (A5) and (A6), we obtain the linearized equation governing (in the case of the *non-Newtonian power-law fluid*) the small perturbations of the LA structure:

$$(D^2 + k^2)(\bar{\eta}(D^2 + k^2)w) - 4k^2 D\left(\frac{\bar{\eta}}{n}Dw\right) + g\frac{D\rho}{p}w = 0. \quad \text{(A7)}$$

Assuming the density and viscosity to be constant within each layer, Eq. (A7) becomes

$$(D^2 + k^2)^2 w - \frac{4k^2}{n}D^2 w = 0. \quad \text{(A8)}$$

Appendix B. Model simplification

To simplify the problem by reducing the number of model variables, the following dimensionless quantities are introduced into the analysis ($i = 1,2,3$; $j = 1,2$):

$$a_i=\frac{\eta_i}{\eta_1+\eta_3},\quad c_i=\frac{\rho_i}{\rho_1+\rho_3},\quad v_1=\frac{\eta_2}{\eta_1}=\frac{a_2}{a_1},\quad v_2=\frac{\eta_2}{\eta_3}=\frac{a_2}{a_3},$$
$$d_i=\frac{h_i}{h_1+h_2},\quad q=k(h_1+h_2),\quad x_j=qd_j=kh_j,$$
$$\lambda=pt_0,\quad \Gamma_j=2\gamma_j t_0,\quad \Im=\frac{(\rho_1+\rho_3)g(h_1+h_2)t_0}{2(\eta_1+\eta_3)},$$
$$\Re_1=\Im c_1 d_1/a_1,\quad \Re_{21}=\Im(c_2-c_1)d_2/a_1,\quad \Re_{32}=\Im(c_3-c_2)d_2/a_3. \tag{A9}$$

Using Eq. (A9) we replace the model variables in the set of ten linear algebraic equations obtained from the boundary conditions (18)–(25) by the dimensionless quantities. It can be proven that a non-trivial solution to the linear algebraic equations exists when the following determinant equals zero:

$$\det\begin{pmatrix} p_{11} & p_{12} & p_{13} & p_{14} & 0 & 0\\ p_{21} & p_{22} & p_{23} & p_{24} & 0 & 0\\ p_{31} & p_{32} & p_{33} & p_{34} & p_{35} & 0\\ p_{41} & p_{42} & p_{43} & p_{44} & p_{45} & p_{46}\\ p_{51} & p_{52} & p_{53} & p_{54} & p_{55} & p_{56}\\ p_{61} & p_{62} & p_{63} & p_{64} & p_{65} & p_{66}\end{pmatrix}=0. \tag{A10}$$

The elements of the matrix $\{p_{ij}\}$ in Eq. (A10) are presented in the form:

$$p_{11}=\lambda\left(\frac{\Re_{21}}{x_2}\tan x_1+\Gamma_1 v_1\right)+\Gamma_1\left(\frac{\Re_{21}}{x_2}(x_1-\tan x_1)+\Gamma_1(1-v_1)x_1\tan x_1\right),$$
$$p_{12}=v_1(\Gamma_1 x_1+(\lambda-\Gamma_1)\tan x_1),\quad p_{13}=\Gamma_1\tan x_1,$$
$$p_{14}=v_1(\Gamma_1 x_1\tan x_1-\lambda),$$
$$p_{21}=\lambda\left(\frac{\Re_{21}}{x_2}x_1+\Re_1+\Gamma_1(1-v_1)x_1\tan x_1\right)+\Re_1\left(\frac{\Re_{21}}{x_2}(x_1-\tan x_1)+\Gamma_1(1-v_1)x_1\tan x_1\right),$$
$$p_{22}=v_1((\Re_1+\lambda)x_1-\Re_1\tan x_1),\quad p_{23}=\Re_1\tan x_1,$$
$$p_{24}=v_1(\Re_1+\lambda)x_1\tan x_1,$$
$$p_{31}=\cosh x_2-x_2\sinh x_2,\quad p_{32}=-\sinh x_2+x_2\cosh x_2,$$
$$p_{33}=-x_2\cosh x_2,\quad p_{34}=x_2\sinh x_2,\quad p_{35}=1,$$
$$p_{41}=x_2\cosh x_2,\quad p_{42}=-x_2\sinh x_2,\quad p_{43}=\cosh x_2+x_2\sinh x_2,$$
$$p_{44}=-\sinh x_2-x_2\cosh x_2,\quad p_{45}=a,\quad p_{46}=b,$$
$$p_{51}=-v_2x_2\sinh x_2,\quad p_{52}=v_2x_2\cosh x_2,$$
$$p_{53}=-v_2(\sinh x_2+x_2\cosh x_2),$$
$$p_{54}=v_2(\cosh x_2+x_2\sinh x_2),$$
$$p_{55}=0.5(a^2-b^2-1)+(v_2\Gamma_1-\Gamma_2)/\lambda,\quad p_{56}=-ab,$$
$$p_{61}=-v_2(\sinh x_2-x_2\cosh x_2),\quad p_{62}=v_2(\cosh x_2-x_2\sinh x_2),$$
$$p_{63}=v_2x_2\sinh x_2,\quad p_{64}=-v_2x_2\cosh x_2,$$
$$p_{65}=0.5a(a^2-3b^2-1/3)+\Re_{32}/(x_2\lambda),\quad p_{66}=0.5b(3a^2-b^2-1/3),$$

where $a=\cos\frac{\varphi}{2}$, $b=\sin\frac{\varphi}{2}$, and $\varphi=\arccos(-1/3)$. Equation (A10) can be reduced to a cubic polynomial function with respect to the growth rate λ of the small perturbations. We do not present here the coefficients of the polynomial function, because their expressions are too cumbersome. We find roots of the cubic polynomial from the Cardano formula (Harris and Stocker, 1998) and consider the maximum positive root for λ, that is, the least stable mode of the RT instability.

References

Adám, A., Panza, G.F., 1989. A critical review of the magnetotelluric information on the upper mantle. Acta Geod. Geoph. Mont. Hung. 24, 395–415.

Anderson, D.L., 2006. Speculations on the nature and cause of mantle heterogeneity. Tectonophysics 416, 7–22.

Anderson, D.L., 2007. New Theory of the Earth, Cambridge University Press.

Anderson, D.L., 2010. Hawaii, boundary layers and ambient mantle-geophysical constraints. J. Petrology, doi: 10.1093/petrology/egq068.

Becker, T.W., 2008. Azimuthal seismic anisotropy constrains net rotation of the lithosphere. Geophys. Res. Lett. 35, L05303.

Bokelmann, G.H., 2002. Which forces drive North America? Geology 30, 1027–1030.

Boschi, L., Ampueroa, J.-P., Peter, D., Maia, P.M., Soldati, G., Giardini, D., 2007. Petascale computing and resolution in global seismic tomography. Phys. Earth Planet. Int. 163, 245–250.

Bostrom, R.C., 1971. Westward displacement of the lithosphere. Nature 234, 356–538.

Calcagnile, G., Panza, G.F., 1987. Properties of the lithosphere–asthenosphere system in Europe with a view toward Earth conductivity. Pure Appl. Geophys. 125, 241–254.

Cathles, L.M., 1975. The Viscosity of the Earth's Mantle. Princeton University Press.

Craig, C.H., McKenzie, D., 1986. The existence of a thin low-viscosity layer beneath the lithosphere. Earth Planet. Sci. Lett. 78 (4), 420–426.

Crespi, M., Cuffaro, M., Doglioni, C., Giannone, F., Riguzzi, F., 2007. Space geodesy validation of the global lithospheric flow. Geophys. J. Int. 168, 491–506.

Cuffaro, M., Doglioni, C., 2007. Global Kinematics in the deep versus shallow hotspot reference frames. In: Foulger, G.R., Jurdy, D.M. (Eds.), Plates, Plumes, and Planetary Processes, Geol. Soc. Am. Spec. Pap., 430, pp. 359–374.

Dingwell, D.B., Courtial, P., Giordano, D., Nichols, A.R.L., 2004. Viscosity of peridotite liquid. Earth Planet. Sci. Lett. 226, 127–138.

Doglioni, C., 1993. Geological evidence for a global tectonic polarity. J. Geol. Soc. 150, 991–1002.

Doglioni, C., Green, D., Mongelli, F., 2005. On the shallow origin of hotspots and the westward drift of the lithosphere. In: Foulger, G.R., Natland, J.H., Presnall, D.C., Anderson, D.L. (Eds.), Plates, Plumes and Paradigms, GSA Sp. Paper, 388, pp. 735–749.

Doglioni, C., Carminati, E., Cuffaro, M., Scrocca, D., 2007. Subduction kinematics and dynamic constraints. Earth Sci. Rev. 83, 125–175.

Dziewonski, A.M., Anderson, D.L., 1981. Preliminary reference Earth model. Phys. Earth Planet. Inter. 25, 297–356.

Fletcher, R.C., 1974. Wavelength selection in the folding of a single layer with power law rheology. Am. J. Sci. 274, 1029–1043.

Green, D.H., Hibberson, W.O., Kovacs, I., Rosenthal, A., 2010. Water and its influence on the lithosphere–asthenosphere boundary. Nature 467, 448–451.

Gripp, A.E., Gordon, R.G., 2002. Young tracks of hotspots and current plate velocities. Geophys. J. Int. 150, 321–361.

Gung, Y., Panning, M., Romanowicz, B., 2003. Global anisotropy and the thickness of continents. Nature 422, 707–710.

Harris, J.W., Stocker, H., 1998. Handbook of Mathematics and Computational Science. Springer, New York.

Heinson, G., 1999. Electromagnetic studies of the lithosphere and asthenosphere. Surveys Geophys. 20 (4), 229–255.

Hirth, G., Kohlstedt, D.L., 1995. Experimental constraints on the dynamics of the partially molten upper mantle, 2, deformation in the dislocation creep regime. J. Geophys. Res. 100, 15441–15449.

Hirth, G., Kohlstedt, D.L., 1996. Water in the oceanic upper mantle: implications for rheology, melt extraction and the evolution of the lithosphere. Earth Planet. Sci. Lett. 144, 93–108.

Hirth, G., Kohlstedt, D.L., 2003. Rheology of the upper mantle and the mantle wedge: a view from the experimentalists. In: John Eiler (Ed.), Inside the Subduction Factory, Geophysical Monograph 138, American Geophysical Union, Washington, DC, pp. 83–105.

Holtzman, B.K., Groebner, N.J., Zimmerman, M.E., Ginsberg, S.B., Kohlstedt, D.L., 2003. Stress-driven melt segregation in partially molten rocks. Geochem. Geophys. Geosyst. 4, 8607.

Ismail-Zadeh, A.T., 1994. Gravitational instability and propagation of tectonic waves in a two-layer model of the upper mantle. In: Chowdhury, D.K. (Ed.), Computational Seismology and Geodynamics, vol. 2. American Geophysical Union, Washington, DC, pp. 76–80.

Ismail-Zadeh, A.T., Tackley, P., 2010. Computational Methods for Geodynamics. Cambridge University Press, Cambridge.

Ismail-Zadeh, A.T., Huppert, H.E., Lister, J.R., 2002. Gravitational and buckling instabilities of a rheologically layered structure: implications for salt diapirism. Geophys. J. Int. 148, 288–302.

Ismail-Zadeh, A., Aoudia, A., Panza, G., 2010. Three-dimensional numerical modeling of contemporary mantle flow and tectonic stress beneath the Central Mediterranean. Tectonophysics 482, 226–236.

Ito, T., Simons, M., 2011. Probing asthenospheric density, temperature, and elastic moduli below the western United States. Science 332, 947–951.

Jin, Z.-M., Green, H.G., Zhou, Y., 1994. Melt topology in partially molten mantle peridotite during ductile deformation. Nature 372, 164–167.

Jordan, T.H., 1974. Some comments on tidal drag as a mechanism for driving plate motions. J. Geophys. Res. 79 (14), 2141–2142.

Kelly, R.K., Kelemen, P.B., Jull, M., 2003. Buoyancy of the continental upper mantle. Geochem. Geophys. Geosyst. 4(2), 1017, doi:10.1029/2002GC000399.

Knopoff, L., Leeds, A., 1972. Lithospheric Momenta and the deceleration of the Earth. Nature 237 (12), 93–95.

Kohlstedt, D.L., Holtzman, B.K., 2009. Shearing melt out of the Earth: an experimentalist's perspective on the influence of deformation on melt extraction. Ann. Rev. Earth Planet. Sci. 37, 561–593.

Kohlstedt, D.L., Zimmerman, M.E., Mackwell, S.J., 2010. Stress-driven melt segregation in partially molten feldspathic rocks. J. Petrol. 51, 9–19.
Korenaga, J., Karato, S.-I., 2008. A new analysis of experimental data on olivine rheology. J. Geophys. Res. 113, B02403.
Kreemer, C., 2009. Absolute plate motions constrained by shear wave splitting orientations with implications for hot spot motions and mantle flow. J. Geophys. Res. 114, B10405.
Le Pichon, X., 1968. Sea-floor spreading and continental drift. J. Geophys. Res. 73 (12), 3661–3697.
Liebske, C., Schmickler, B., Terasaki, H., Poe, B.T., Suzuki, A., Funakoshi, K., Ando, R., Rubie, D.C., 2005. Viscosity of peridotite liquid up to 13 GPa: implications for magma ocean viscosities. Earth Planet. Sci. Lett. 240, 589–604.
Marone, F., Romanowicz, B., 2007. The depth distribution of azimuthal anisotropy in the continental upper mantle. Nature 447, 198–202.
Mei, S., Bai, W., Hiraga, T., Kohlstedt, D.L., 2002. Influence of melt on the creep behavior of olivine-basalt aggregates under hydrous conditions. Earth Planet. Sci. Lett. 201, 491–507.
Moore, G.W., 1973. Westward tidal lag as the driving force of plate tectonics. Geology 1, 99–100.
Nelson, T.H., Temple, P.G., 1972. Mainstream mantle convection; a geologic analysis of plate motion. AAPG Bulletin 56, 226–246.
O'Connell, R., Gable, C.G., Hager, B., 1991. Toroidal-poloidal partitioning of lithospheric plate motions. In: Sabadini R. et al. (Eds.), Glacial Isostasy, Sea-Level and Mantle Rheology, vol. 334, Kluwer Academic Publisher, pp. 535–551.
Panza, G., Raykova, R.B., Carminati, E., Doglioni, C., 2007a. Upper mantle flow in the western Mediterranean. Earth Planet. Sci. Lett. 257, 200–214.
Panza, G.F., Peccerillo, A., Aoudia, A., Farina, B., 2007b. Geophysical and petrological modeling of the structure and composition of the crust and upper mantle in complex geodynamic settings: the Tyrrhenian Sea and surroundings. Earth Sci. Rev. 80, 1–46.
Panza, G., Doglioni, C., Levshin, A., 2010. Asymmetric ocean basins. Geology 38, 59–62.
Paulson, A., Zhong, S., Wahr, J., 2007. Limitations on the inversion for mantle viscosity from postglacial rebound. Geophys. J. Int. 168, 1195–1209.
Pollitz, F.F., Burgmann, R., Romanowicz, B., 1998. Viscosity of oceanic asthenosphere inferred from remote triggering of earthquakes. Science 280, 1245–1249.
Ranalli, G., 2000. Westward drift of the lithosphere: not a result of rotational drag. Geophys. J. Int. 141, 535–537.
Ricard, Y., Doglioni, C., Sabadini, R., 1991. Differential rotation between lithosphere and mantle: a consequence of lateral viscosity variations. J. Geophys. Res. 96, 8407–8415.
Riguzzi, F., Panza, G., Varga, P., Doglioni, C., 2010. Can Earth's rotation and tidal despinning drive plate tectonics? Tectonophysics 484, 60–73.
Romanowicz, B., 2003. Global mantle tomography: progress status in the last 10 years. Annu. Rev. Geoph. Space Phys., 31(1), 303.
Rychert, C.A., Fischer, C.M., Rondenay, S., 2005. A sharp lithosphere–asthenosphere boundary imaged beneath eastern North America. Nature 436, 542–545.
Scoppola, B., Boccaletti, D., Bevis, M., Carminati, E., Doglioni, C., 2006. The westward drift of the lithosphere: a rotational drag? Bull. Geol. Soc. Am. 118, 199–209.
Smith, R.B., 1979. The folding of a strongly non-Newtonian layer. Am. J. Sci. 279, 272–287.
Stevenson, D.J., 1994. Weakening under stress. Nature 372, 129–130.
Thybo, H., 2006. The heterogeneous upper mantle low velocity zone. Tectonophysics 416, 53–79.
Waldhauser, F., Lippitsch, R., Kissling, E., Ansorge, J., 2002. High-resolution teleseismic tomography of upper-mantle structure using an a priori three-dimensional crustal model. Geophys. J. Int. 150, 403–414.
Zandt, G., Gilbert, H., Owens, T.J., Ducea, M., Saleeby, J., Jones, C.H., 2004. Active foundering of a continental arc root beneath the southern Sierra Nevada in California. Nature 431, 41–46.